ACADEMIA ROMÂNĂ
Revue Roumaine de Chimie
https://www.icf.ro/rrch/

Rev. Roum. Chim.,
2023, *68*(9), 463–471
DOI: 10.33224/rrch.2023.68.9.07

SYNTHESIS AND CHARACTERIZATION OF NOVEL THIOSEMICARBAZIDE FOR NONLINEAR OPTICAL APPLICATIONS: COMBINED EXPERIMENTAL AND THEORETICAL STUDY

Djebar HADJI,[a,b*] Abdelmadjid BENMOHAMMED,[c,d] Younes MOUCHAAL[e,f] and Ayada DJAFRI[d]

[a] Laboratory of Modeling and Calculation Methods, University of Saïda - Dr. Moulay Tahar, 20000 Saïda, Algeria
[b] Department of Chemistry, Faculty of Sciences, University of Saïda - Dr. Moulay Tahar, 20000 Saïda, Algeria
[c] Department of Chemistry, Faculty of Exact Sciences, University of Mascara, Mascara, Algeria;
[d] Laboratory of Applied Organic Synthesis (LSOA), Department of Chemistry, Faculty of Exact and Applied Sciences, Oran1 Ahmed Ben Bella University, BP 1524 El M'naouer, Oran, Algeria
[e] Department of Physics, Faculty of Exact Sciences, University of Mascara, Mascara, Algeria
[f] Laboratory of Thin Films Physics and Materials for Electronics (LPCMME); Oran University1 Ahmed Ben Bella, BP 1524 El M'naouer, Oran, Algeria

Received January 5, 2023

(E)-4-(4-methoxyphenyl)-1-((E)-3(2nitrophenyl) allylidene) thiosemicarbazide was synthesised and screened for nonlinear optical properties. The novel compound has been characterized by infrared spectroscopy, ^{1}H and ^{13}C nuclear magnetic resonance. The experimental and theoretical optical gap energy is obtained using the Tauc method and density functional theory and has been estimated to be around 2.72 and 2.69 eV, respectively. The synthesized thiosemicarbazide exhibits efficiency hyper-Rayleigh scattering hyperpolarizability is calculated to be 6794.51 a.u. at the PBE0 functional. A direct relationship of the hyper-Rayleigh scattering hyperpolarizability with the optical band gap and between the hyper-Rayleigh scattering hyperpolarizability and electric field-induced second harmonic generation is found. The study showed the potential of the novel thiosemicarbazide as nonlinear optical candidates.

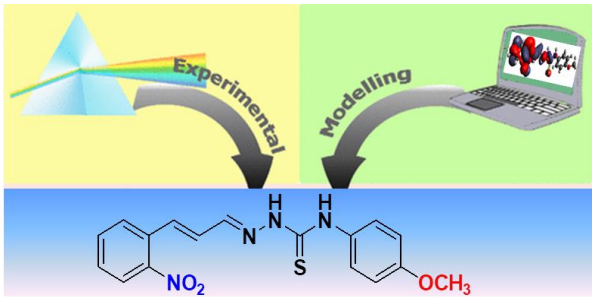

INTRODUCTION

Organic compounds have received particular attention due to their nonlinear optical (NLO) properties,[1–4] as they are widely used in the large and important field of information and telecommunications technologies, in particular dynamic image processing, optical computing, and optical communication.[5–7] In nonlinear optics, thiosemicarbazone-based derivatives are widely studied by experimental and theoretical communities due to their low dielectric constants, ultrafast and broadband electronic responses considered in promising optoelectronic technologies.[8,9] In this work, the aim was to synthesis, characterize, calculate, and analyze the

* Corresponding author: hadji120780@yahoo.fr ; djeber.hadji@univ-saida.dz

polarizability and first-order hyperpolarizability of a novel (E)-4-(4-methoxyphenyl)-1-((E)-3(2nitrophenyl) allylidene) thiosemicarbazide (MPNPAT). We performed theoretical calculations using five density functional theory (DFT) levels (B3LYP, PBE0, CAM-B3LYP, ωB97X-D, and M06-2X). This study will firstly focus on the relation between the higher hyper-Rayleigh scattering (HRS) hyperpolarizability β_{HRS} and the electric field-induced second harmonic generation (EFISHG) $\beta_{//}$, and the relation between the first hyperpolarizability β and the energy gaps of this compound. We also investigated the frontier molecular orbitals (HOMO and LUMO), their energies, the location, and the nature of the isosurfaces of these frontier orbitals.

EXPERIMENTAL

1. Materials

The chemicals used in the syntheses were obtained from Aldrich Chemical Company and were used without further purification. Melting points were determined on Büchi B-540 apparatus and are uncorrected. IR spectra were taken on Perkin-Elmer Spectrum two FT-IR spectrometer and the reported wave numbers are given in cm^{-1}. The optical measurements were carried out at room temperature using an ultraviolet-visible (UV-vis) spectro-photometer (Perkin-Elmer Lambda 950 UV-vis-near-IR with integrating sphere with a scan rate of 60 nm/min (lamp changes at 326 nm). The optical transmission was measured in [300,1100] wave length range. ^{1}H nuclear magnetic resonance (NMR) spectra were recorded on a BRUKER AC 300P (300 MHz) spectrometer (Bruker, Bremen, Germany), ^{13}C-NMR spectra on a BRUKER AC 300 P (75 MHz, Bruker) spectrometer in DMSO-d_6. The ^{1}H-NMR chemical shifts were reported as parts per million downfield from tetramethylsilane (Me_4Si), and the ^{13}C-NMR chemical shifts were referenced to the solvent peaks: DMSO-d_6 (39.6 ppm). Silica gel 60 (Merck, 230–400 mesh) was used for column chromatography: Thin-layer chromatography was performed with silica gel Merck 60F-254 (0.25 mm layer thickness).

Synthesis of the (E)-4-(4-methoxyphenyl)-1-((E)-3(2nitrophenyl) allylidene) thiosemicarbazide

To a solution of 4-methoxyphenyl-3-thiosemicarbazide (0.4 g, 2 mmol) in absolute ethanol (20 ml) were added the 2-nitro cinnamaldehyde (0.354 g, 2 mmol) and acetic acid (0.5 mL). Reaction mixture was stirred at reflux temperature for 3 h, and then cooled to room temperature (Scheme 1). The precipitate was filtered and recrystallized from ethanol.

(E)-4-(4-methoxyphenyl)-1-((E)-3(2nitrophenyl) allylidene) thiosemicarbazide

Yield: 90%. m.p. 164 °C. FTIR (ATR, νmax., cm^{-1}): 3206 and 3105 (NH), 2974 (C-H, aliphatic); 1496 (C=N), 1341, 812 (aromatic, NO_2), 1238 (C=S), ^{1}H-NMR (300 MHz, DMSO-d_6): δ (ppm): δ 3.76 (s, 3H, OCH_3), 6.90 (d, 2H, *J* = 9 Hz, Ar-H), 6.97 (dd, 1H, *J* = 16.0 Hz, *J* = 9.26 Hz, =CH), 7.29 (d, 1H, *J* = 16 Hz, =CH), 7.43 (d, 2H, *J* = 9 Hz, Ar-H), 7.59 (t, 1H, *J* = 7.24 Hz, Ar-H), 7.76 (d, 2H, *J* = 7.61 Hz, Ar-H), 7.9-8.03 (m, 2H, Ar-H), 9.87 (s, 1H, NH), 11.84 (s, 1H, NH); ^{13}C-NMR (75 MHz, DMSO-d_6): δ (ppm): 55.7 (OCH_3), 113.80 (2CH), 125.16 (CH), 127.16 (2CH), 128.5 (CH), 130.04 (CH), 130.31 (CH), 131.0 (C), 132.23 (C), 133.12 (CH), 134.12 (C), 144.11 (CH), 148.23 (CH), 157.28 (C), 176.5 (C=S).

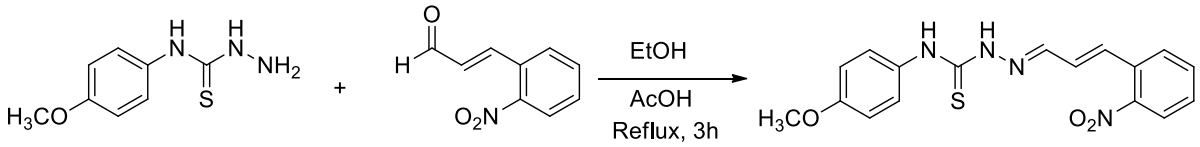

Scheme 1 – Synthetic scheme of MPNPAT.

2. Characterization

IR spectral analysis

The infrared (IR) spectrum of our compound was recorded in the solid state using the ATR technique. The IR spectra gave important information about the skeleton of structures. The band obtained at 1496 cm^{-1} is due to the formation of imine group (C=N) between aldehyde and amine.[10,11] The NH stretching vibrations were observed at 3206 and 3105 cm^{-1}, respectively. The significant strong absorption peak of C=S and the free aliphatic CH group appeared in the 1238 and 2947 cm^{-1} (Fig. S1), respectively. The absence of band around 2600–2800 cm^{-1} (SH) in the IR indicates that the ligand exists in the thione form [12] -NO_2 stretching vibration is recorded at 1340 and 812 cm^{-1}. The results of the preliminary analysis by IR spectroscopy of both compounds are in agreement with those obtained for the same type of compounds.[13,14]

^{1}H-NMR and ^{13}C-NMR spectra

The signal of the protons of the -OCH_3 group resonates in the form of a singlet at 3.76 ppm. The signal of N=CH shows a doublet at δ_H = 7.87–7.90 ppm because of the anisotropy of the N (sp^2) atom,[15] The ^{1}H-NMR spectrum of the thiosemicarbazone shows two doublets at δ_H = 6.97–7.05 ppm because of (CH=CH) (Fig. S2 from the supplementary materials SI), whereas N-H thiourea protons are found at 9.87 and 11.84 ppm for N-H adjacent to the monosubstituted phenyl ring and for N-H adjacent to the CH=N moiety, respectively. The synthesized MPNPAT is of *E* configuration, which was confirmed using ^{1}H-NMR spectroscopy, as the signal of the NH group was in the range of 9-12 ppm, compared to the Z isomer, which has a characteristic NH signal in the range of 14–15 ppm.[16]

The chemical shift of the azomethine group (C=N) appeared at 144.11 ppm, while for the C=S group, it occurred

at 176.50 ppm (Fig. S3), both comparable to the literature.[17,18] The values between 125.15 to 128.49 ppm correspond to the sp2 carbon of CH=CH (cynnamaldehyde),[14]

Optical properties

The UV-vis spectrum of the studied compound gives information about the optical deviation band. It also provides information about the optical band gap (E_g). The E_g of insulators is higher than (4 eV) while for semiconductor is less than 3 eV.[19] In this part of the study, the E_g is calculated from the UV-vis spectrum (Fig. 1).

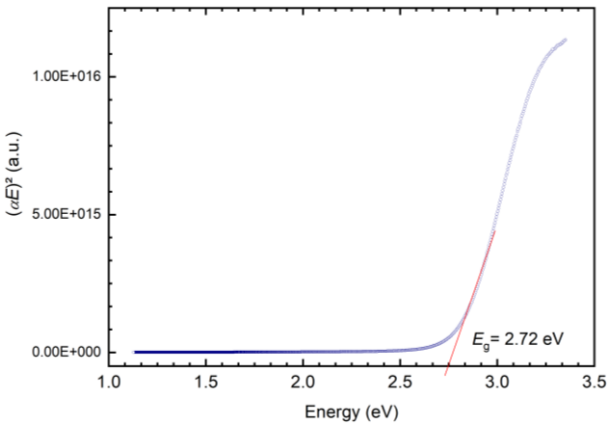

Fig. 1 – Variation of $(\alpha hv)^2$ value of MPNPAT with respect to incident light energy.

Figure 1 shows the evolution curves of αhv of the synthesized compound as a function of the incident photon energy. The E_g of the studied compound can be deduced from interaction with the incident photon energy Tauc equation:[20]

$$\alpha hv = (hv - E_g)^{1/2} \quad (1)$$

where α is the absorption coefficient, h is Planck's constant, v is the photon frequency, and E_g is the band gap energy. The absorption coefficient is obtained from Lambert's formula:

$$\alpha = (1/T)\log(1/T) \quad (2)$$

The E_g values were evaluated based on the linearization of Eq. 1, by the extrapolation of the $(\alpha hv)^2$ as a function of the hv curve. The estimated E_g for the MPNPAT was 2.72 eV. This E_g value suggests that the MPNPAT is a semiconductor and is in the same range of highly efficient photovoltaic materials. Thus, this compound could be considered as a potential material for harvesting solar radiation in solar cell applications.[21]

RESULTS AND DISCUSSION

1. Computational details

The optimized geometry of the MPNPAT has been performed using the B3LYP functional[22] together with the 6-311++G(d,p) basis set[23–25] implemented in Gaussian 09 package of programs. The optimized geometry represents an isolated molecule under ideal conditions with a stationary point at the potential energy surface. The visualization of MPNPAT optimized structure, HOMO, and LUMO plots have been carried out using GaussView 5.1 program. The MPNPAT final geometry was showed in Fig. 2.

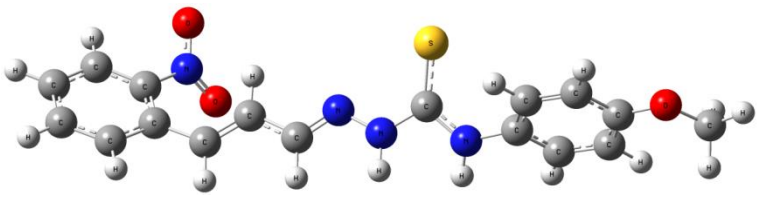

Fig. 2 – The MPNPAT optimized structure at the B3LYP/6-311++G(d,p) level.

The electrical properties such as the dipole moment μ, mean polarizability $\langle\alpha\rangle$, polarizability anisotropy $|\alpha|$, total first hyperpolarizability β_{tot}, electric-field-induced second harmonic generation (EFISHG) $\beta_{//}$, and the hyper-Rayleigh scattering (HRS) first hyperpolarizability β_{HRS} are calculated for the optimized MPNPAT geometry. The obtained β components show that the β ones along the $x-$axis are the majority. Figure 3 showed that the MPNPAT structure is placed on the $xy-$plane. Several DFT levels B3LYP, PBE0,[26] CAM-B3LYP,[27] ωB97X-D,[28] and M06-2X[29,30] have employed for calculation. According to theoretical study,[31] the DFT XC functionals give accurate linear and NLO results. The total dipole moments are defined as follows:

$$\mu = \sqrt{(\mu_x^2 + \mu_y^2 + \mu_z^2)} \quad (3)$$

The $\langle\alpha\rangle$ was calculated from α components as:[32]

$$\langle\alpha\rangle = \frac{1}{3}\sum_{i=x,y,z}\alpha_{ii} \quad (4)$$

$$\langle\alpha\rangle = \frac{1}{3}(\alpha_{xx} + \alpha_{yy} + \alpha_{zz}) \quad (5)$$

and the $\Delta\alpha$ is:

$$|\alpha| = \sqrt{\frac{1}{2}\left((\alpha_{xx} - \alpha_{yy})^2 + (\alpha_{xx} - \alpha_{zz})^2 + (\alpha_{yy} - \alpha_{zz})^2\right)} \quad (6)$$

For the first hyperpolarizability β, we are interested on $\beta_{//}$ and β_{HRS}. The $\beta_{//}$ is the central

quantity of β vector projected along the μ-axis and calculated using the following formula;[33]

$$\beta_{\underline{\ }}(-2\omega,\omega,\omega) = \beta_{\underline{\ }} = \frac{1}{5}\sum_{i}\frac{\mu_i}{|\vec{\mu}|}\sum_{j}(\beta_{ijj}+\beta_{jij}+\beta_{jji}) \quad (7)$$

In the static limits ($\beta_{ijj} = \beta_{jij} = \beta_{jji}$), $\beta_{//}$ becomes

$$\beta_{//} = \frac{3}{5}\sum_{i=x,y,z}\frac{\mu_i\beta_i}{|\vec{\mu}|} \quad (8)$$

$|\vec{\mu}|$ is the norm of the dipole moment, μ_i and β_i the i^{th} components of μ and β vectors, respectively. The β_{HRS} is related to the HRS intensity for nonpolarized incident light of frequency ω, and observation of plane-polarized scattered light made perpendicular to the propagation plane. The full β_{HRS} is described by

$$\beta_{HRS} = \langle\beta^2_{HRS}\rangle = \langle\beta^2_{ZZZ}\rangle + \langle\beta^2_{ZXX}\rangle \quad (9)$$

$$DR = \frac{I^{2\omega}_{VV}}{I^{2\omega}_{HV}} = \frac{\langle\beta^2_{ZZZ}\rangle}{\langle\beta^2_{ZXX}\rangle} \quad (10)$$

$\langle\beta^2_{ZZZ}\rangle$ and $\langle\beta^2_{ZXX}\rangle$ given by the molecular (x, y, z) reference are averages of β tensor components that describe the isotropic distribution of molecular orientations in dilute solutions. The $\langle\beta^2_{ZZZ}\rangle$ and $\langle\beta^2_{ZXX}\rangle$ were calculated without assuming Kleinman's conditions, and the temperature convention was used for defining the β quantities. The full $\langle\beta^2_{ZZZ}\rangle$ and $\langle\beta^2_{XZZ}\rangle$ expressions can be find in SI and in Ref.[34]

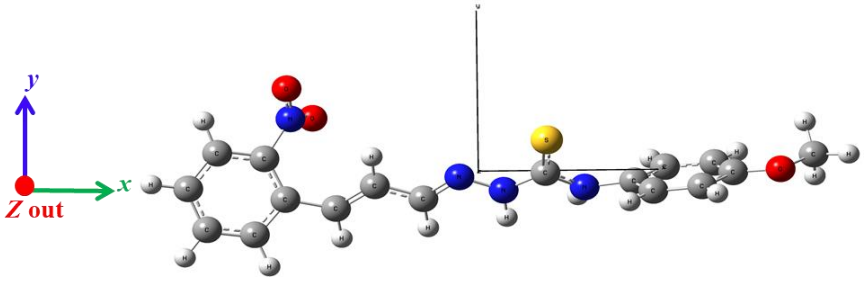

Fig. 3 – The MPNPAT orientation during calculations.

2. Dipole moment

The purpose of this study is to show that μ, α, and β can be calculated in an effective and efficient manner with the proper choice of DFT functionals. For this, we used the B3LYP, PBE0, CAM-B3LYP, ωB97X-D, and M05-2X levels of theory. Table 1 displays the μ values computed at several DFT levels, and the total dipole moment vector of our MPNPAT was showed in Fig. 4. The obtained results are compared with the corresponding theoretical and experimental μ values for similar compounds.[35] Inspection of Table 1 shows that the PBE0 functional gives closed μ value (7.56 D) compared to obtained μ value (7.47 D) of the similar salicylaldehyde thiosemicarbazone.[36] We recall that a difference of about 0.01 to 1 a.u. is typical in such calculations. The obtained μ values of the MPNPAT are ranged between 7 and 8 D using the PBE0 and M05-2X functionals, respectively. High μ value equal to 8.17 D is obtained using the M05-2X level of theory, while the lowest μ value equal to 7.56 D is obtained at the PBE0 level. Compared to the urea (1.37 D);[37] the extent of μ of our MPNPAT is found to be larger. Overall, the μ values order was observed to be $\mu_{M05\text{-}2X} > \mu_{CAM\text{-}B3LYP} > \mu_{\omega B97X\text{-}D} > \mu_{B3LYP} > \mu_{PBE0}$. Using DFT methods, recent study[35] showed that the dipole moment of similar thiosemicarbazones are ranged from 7 to 8 D like our compound. A greater magnitude of the dipole moment of thiosemicarbazone molecules than the urea molecule (1.37 D).

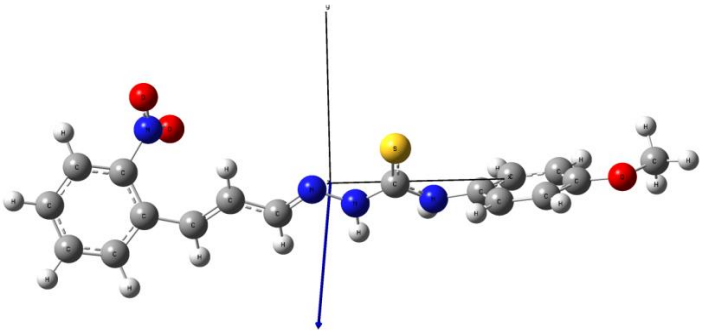

Fig. 4 – The total dipole moment vector of our MPNPAT.

Table 1

μ in D, $\langle\alpha\rangle$, $|\alpha|$, $\beta_{//}$, β_{HRS} in a.u., and DR of the MPNPAT obtained using five DFT functionals at the 6-311++G(d,p) basis set (comparisons with M06 values for similar thiosemicarbazide are made)

	μ	$\langle\alpha\rangle$	$\lvert\alpha\rvert$	$\beta_{//}$	β_{HRS} **(DR)**
B3LYP	7.90	337.65	370.48	–31.01	3076.58 (5.00)
PBE0	7.56 7.74 [a]	366.21	444.15	–665.54	6794.51 (5.00)
CAM-B3LYP	8.14	314.15	313.14	–13.25	1485.58 (5.01)
ωB97X-D	8.13	312.60	311.37	–36.03	1338.56 (5.00)
M05-2X	8.17	311.57	314.58	–31.44	1540.01 (5.01)

[a] M06/6-311G(d,p) results for salicylaldehyde thiosemicarbazide.[35]

3. Polarizability

In order to investigate the accuracy of our polarizability calculations and disclose the structure-polarizability relationship, we have computed $\langle\alpha\rangle$ and $|\alpha|$ using the B3LYP, PBE0, CAM-B3LYP, ωB97X-D, and M05-2X functionals at the 6-311++G(d,p) basis set. The α results are presented in Table 1. The presented α values show that $\langle\alpha\rangle$ values for our novel MPNPAT is observed to be 337.65, 366.21, 314.15, 312.60, and 311.57 a.u. at B3LYP, PBE0, CAM-B3LYP, ωB97X-D, and M05-2X, respectively. For $|\alpha|$, the presented values is observed to be 370.48, 444.15, 313.14, 311.37, and 314.58 a.u. at the B3LYP, PBE0, CAM-B3LYP, ωB97X-D, and M05-2X, respectively. The greater $\langle\alpha\rangle$ value (366.21 a.u.) is noticed using the PBE0 level of theory, while the M05-2X exhibits the lowest $\langle\alpha\rangle$ value (311.57 a.u.). In the same task, and like $\langle\alpha\rangle$, the PBE0 gives the high $|\alpha|$ value (444.15 a.u.). The ωB97X-D gives the lowest value (311.37 a.u.). The same assessment has been obtained in several studies.[3,37,38] In our studies[38,39] for $\langle\alpha\rangle$ and $|\alpha|$ of (Z)-5-benzylidene-3-N(4-methylphenyl)-2-thioxothiazolidin-4-one[38] and 2-thioxo-3-N, (4-methylphenyl) thiazolidine-4-one,[39] we showed that the Perdew-Burke-Ernzerhof (PBE0) with a Hartree-Fock (HF) contribution of 25% is the most satisfied functional for calculating $\langle\alpha\rangle$ and $|\alpha|$ of rhodanines. It was showed that the PBE0 level which included to GGA functionals for DFT polarizability calculations gives rightly results compared to other DFT levels methods. According to the DFT levels used in this study; the order of $\langle\alpha\rangle$ and $|\alpha|$ for our new MPNPAT is found to be in the following decreasing order at:

$\langle\alpha\rangle$ $\quad \langle\alpha\rangle_{\mathrm{PBE0}} > \langle\alpha\rangle_{\mathrm{B3LYP}} > \langle\alpha\rangle_{\mathrm{CAM\text{-}B3LYP}} > \langle\alpha\rangle_{\mathrm{\omega B97X\text{-}D}} > \langle\alpha\rangle_{\mathrm{M05\text{-}2X}}$

$|\alpha|$ $\quad |\alpha|_{\mathrm{PBE0}} > |\alpha|_{\mathrm{B3LYP}} > |\alpha|_{\mathrm{M05\text{-}2X}} > |\alpha|_{\mathrm{CAM\text{-}B3LYP}} > |\alpha|_{\mathrm{\omega B97X\text{-}D}}$.

4. Second-order NLO responses

In this study, one of our aims is to focus on theoretically evaluating the second order NLO behaviour ($\beta_{//}$, β_{HRS}, and DR) of MPNPAT using B3LYP, PBE0, CAM-B3LYP, ωB97X-D, and M05-2X levels of theory. The results are displayed in Table 1 and Fig. 5. Among all functionals used in this study, a higher β_{HRS} value is examined in MPNPAT to be 6794.51 a.u. obtained using the PBE0 level. The B3LYP level shows also a high β_{HRS} value up to 3076.58 a.u. These functionals (B3LYP and PBE0) include a minor fraction of HF exchange (20% and 40%), respectively. On the other hand, the CAM-B3LYP and ωB97X-D give the lowest β_{HRS} values varied between 1338.56 and 1485.58 a.u. The CAM-B3LYP and ωB97X-D functionals containing larger amounts of HF exchange. The M05-2X functional with 56% HF exchange, gives medium β_{HRS} value equal to 1540.01 a.u. Recent experimental and theoretical studies[40–43] show the suitability of thiosemicarbazide derivatives in NLO applications.

The presence of the -OCH_3 donor and -NO_2 groups in both sides of our novel compound produce large hyperpolarizability. As regards to the π-electron donating capacity, the -OCH_3 is small donor groups compared to other strong donor groups with N heteroatom like -NH_2 and -$NHNH_2$,[44] but the presence of strong acceptor -NO_2 with -OCH_3 which results charge transfer (CT) across our MPNPAT. According to Oudar *et al.*,[45] the greater the CT, the larger the NLO properties. Mermer *et al.*,[40] showed high hyperpolarizability values of thiosemicarbazide derivatives and their Cu(II) complexes. In other experimental and DFT study,[41]

the β value (7.1223×10^{-30} esu) of (E)-1-(4-bromobenzylidene)semicarbazide is nineteen times greater than the value of urea (0.372×10^{-30} esu) which confirm the high β value of these thiosemicarbazide derivatives. For this class of compounds, the second-order hyperpolarizability $< \gamma >$ are also studied using DFT[42] and Z-scan analysis.[46] The authors[42] showed that μ, α, and γ of the studied chromone-based thiosemicarbazide derivatives are larger in contrast to the reference molecule.[42] For our thiosemicarbazide, opposite variations were obtained between $\beta_{//}$ and β_{HRS} (Fig. 5 and Table 1). The PBE0 and CAM-B3LYP levels give the smallest and the largest $\beta_{//}$ values, respectively. From this standpoint, the β_{HRS} and $\beta_{//}$ order was established as follows:

$$\beta_{\mathrm{HRS}\ \omega\mathrm{B97X\text{-}D}} < \beta_{\mathrm{HRS}\ \mathrm{CAM\text{-}B3LYP}} < \beta_{\mathrm{HRS}\ \mathrm{M05-2X}} < \beta_{\mathrm{HRS}\ \mathrm{B3LYP}} < \beta_{\mathrm{HRS}\ \mathrm{PBE0}}$$

$$\beta_{//\ \mathrm{CAM-B3LYP}} > \beta_{//\ \mathrm{B3LYP}} > \beta_{//\ \mathrm{M05-2X}} > \beta_{//\ \omega\mathrm{B97X\text{-}D}} > \beta_{//\ \mathrm{PBE0}}$$

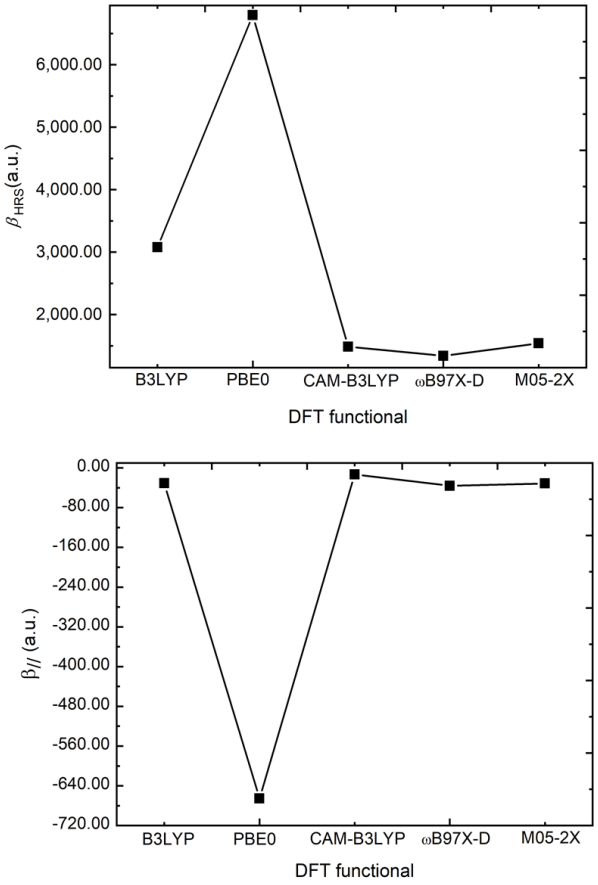

Fig. 5 – β_{HRS} (upper panel) and $\beta_{//}$ (lower panel) of the MPNPAT determined at five DFT levels.

The NLO properties of ((E)-1-(3,5 dibromo benzylidene) semicarbazide[45] have been evaluated by first-order hyperpolarizability studies. The calculated β_{tot} of the semicarbazide derivative (1.29×10^{-30} esu) is larger than that (0.1947×10^{-30} esu) of urea. The authors[43] showed that the high β_{tot} value is attributed to the CT exiting amid the aromatic rings within the semicarbazide derivative, and revealed the NLO property of the compound. The DR $= \frac{\langle\beta^2_{\mathrm{ZZZ}}\rangle}{\langle\beta^2_{\mathrm{ZXX}}\rangle}$ gives the shape information on the compound geometry, the part of the molecule responsible for the NLO response. In our MPNPAT, the DR value is exactly equal to 5 (DR = 5) obtained at B3LYP, PBE0, CAM-B3LYP, ωB97X-D, and M05-2X levels, which are congruent with the topology of one-dimensional system.

5. Frontier molecular orbitals (FMOs) analysis

In this part, the E_{HOMO}, E_{LUMO}, and their HOMO-LUMO energy gap ($\Delta\varepsilon$) have been calculated and their isosurfaces HOMO and LUMO are presented and analysed in detail using the B3LYP, CAM-B3LYP, M05-2X, PBE0, and ωB97X-D. In Table 2, Fig. 6, and Fig. 9 we

presented all these results. The $\Delta\varepsilon$ plays a crucial role in the chemical stability of compounds and for determining electrical properties.[47] The calculated $\Delta\varepsilon$ values of the MPNPAT are ranged from 1.47 to 6.81 eV using the PBE0 and ωB97X-D levels of theory, respectively. The B3LYP give good results compared to the experimental values obtained using the UV-vis measurement. Our study showed that the β_{HRS} displays an inverse relationship with $\Delta\varepsilon$, high β_{HRS} has been obtained at lower $\Delta\varepsilon$ (Fig. 6). Excellent agreement has been obtained in earlier studies.[48–50]

Table 2

E_{HOMO}, E_{LUMO}, and $\Delta\varepsilon$ in eV, and the β_{HRS} and $\beta_{//}$ in a.u. of the MPNPAT obtained using five DFT levels at the 6-311++G(d,p) basis set (comparisons with experiment are made)

	E_{HOMO}	E_{LUMO}	$\Delta\varepsilon$	$\beta_{//}$	β_{HRS}
B3LYP	–5.68	–2.72	2.69	-31.01	3076.58
PBE0	–4.79	–3.32	1.47	-665.54	6794.51
CAM-B3LYP	–7.14	–1.49	5.65	-13.25	1485.58
ωB97X-D	–7.68	–0.87	6.81	-36.03	1338.56
M05-2X	–7.10	–1.67	5.43	-31.44	1540.01
Exp			2.72		

Compared to PBE0, CAM-B3LYP, ωB97X-D, and M05-2X functionals; the B3LYP/6-311++G(d,p) level was found to give the best match with the experimental $\Delta\varepsilon$ at 2.72 eV. This experimental $\Delta\varepsilon$ value is measured by UV-vis (Fig. 1). Combined experimental and DFT study of amorphous covalent inorganic-organic hybrid frameworks showed by Basharat *et al.*[51] that the B3LYP/6-311+G(d,p) level gives closed Δε values with the experimental ones. The general trend in our calculated $\Delta\varepsilon$ is ωB97X-D > CAM-B3LYP > M05-2X > B3LYP > PBE0. The PBE0 functional gives also close $\Delta\varepsilon$ value (1.47 eV) compared to CAM-B3LYP, ωB97X-D, and M05-2X levels. The suitability of the PBE0 to predict reliable $\Delta\varepsilon$ value is confirmed in recent theoretical and experimental studies.[44–47] The low Δε value obtained at the PBE0 level endorses the potential of the MPNPAT as organic semiconductor. Like our novel MPNPAT; salicylaldehyde thiosemicarbazone derivatives with a low $\Delta\varepsilon$ and high β are useful for NLO applications.[35] Khalid *et al.*[35] showed that the salicylaldehyde thiosemicarbazone derivatives get average total hyperpolarizability values varied between 269 to 508 a.u. calculated at the M06/6-311G(d,p) level. The authors show that the smaller $\Delta\varepsilon$ of molecules indicated the possibilities of intramolecular CT, and their good reactivity.

Using the B3LYP, PBE0, CAM-B3LYP, ωB97X-D, and M05-2X levels of theory; the FMOs analysis showed that the HOMO is delocalized on the cycle which carries the methoxy group (Fig. 7). The delocalization is expanded on the S-linked atoms. The same assessment has been showed by Basri *et al.*[56] on their study of chromone-based thiosemicarbazone derivatives. While the LUMO electron density is principally delocalized over the whole cycle which carries the -NO_2 group (Fig. 7). Indeed, intramolecular CT from the HOMO to the LUMO is possible, hence providing suitable reasons to utilize this thiosemicarbazone in CT related phenomenon like NLO properties.

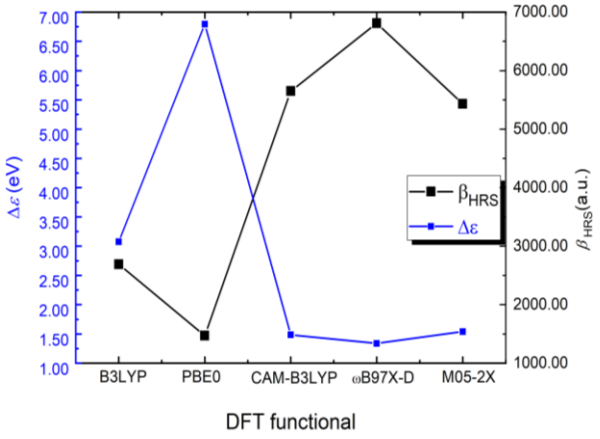

Fig. 6 – β_{HRS} in a.u. and the Δε in eV for MPNPAT estimated at five DFT functionals.

Due to their easy synthesis, structural modifications, facile manufacturing, and less cost like our new MPNPAT, similar thiosemicarbazones facile synthetised are studied also by Khalid *et al.*,[35] the authors showed that these thiosemicarbazones has potentially active in nonlinear optic due to their high calculated first and second hyperpolarizavbility values. The obtained $\Delta\varepsilon$ values of similar thiosemicarbazones are ranged from 3 to

5 eV.[56] On the other hand, our obtained $\Delta\varepsilon$ values are ranged from 2 to 6 eV, which show that our MPNPAT gets low $\Delta\varepsilon$ value compared to the studied thiosemicarbazones by Basri *et al.*[56]

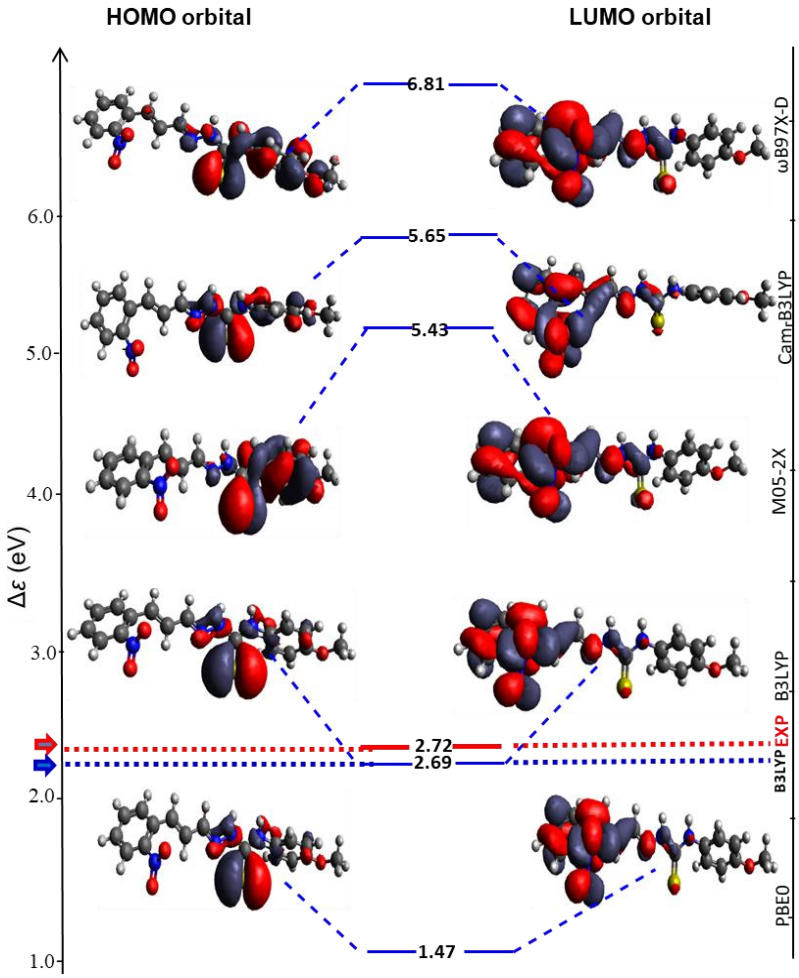

Fig. 7 – HOMO and LUMO of the MPNPAT and their $\Delta\varepsilon$ (in eV) estimated by five DFT functionals at the 6-311++G(d,p) basis set.

CONCLUSIONS

In summary, this paper describes the synthesis, characterization, linear and NLO properties of novel MPNPAT. This new thiosemicarbazide was produced in one-step process with good to excellent yields. The UV-vis and DFT comparative analysis indicated the good agreement between optical bond gaps. The second-order optical nonlinearity calculation was carried out, and the HRS hyperpolarizability was 6794.51 a.u. The DR value (DR = 5) obtained is congruent with the topology of one-dimensional system. Opposite correlation between the β_{HRS} and energy gap has been obtained. The NLO calculations suggest that the novel thiosemicarbazone gets efficient HRS hyperpolarizability responses considered in promising NLO materials. It is inferred that investigated ferrocene-based thiosemicarbazide derivatives[57,58] may have prospective applications in development of novel NLO materials based on thiosemicarbazide derivatives.

Acknowledgements. This work was supported by the Algerian ministry of higher education and scientific research as well as the general directorate of scientific research and technological development.

REFERENCES

1. D. Hadji and A. Rahmouni, *Med. J. Chem.*, **2015**, *4*, 185.
2. D. Hadji, A. Rahmouni, D. Hammoutène and O. Zekri, *J. Mol. Liq.*, **2019**, *286*, 110939.
3. A. Kenane, D. Hadji, K. Argoub, A. Yahiaoui, A. Hachemaoui, K. Toubal, A. M. Benkouider, O. Rasoga,

A. Stanculescu and A. C. Galca, *J. Elec. Mater.*, **2023**, *52*, 530–539.
4. F. Yahia Cherif, D. Hadji and N. Benhalima, *Phys. Chem. Res.*, **2023**, *11*, 33–48.
5. E. M. Breitung, C. F. Shu and R. J. McMahon, *J. Am. Chem. Soc.*, **2000**, *122*, 1154–1160.
6. R. D. Miller, D. M. Burland, M. Jurich, V. Y. Lee, C. R. Moylan, J. I. Thackara and W. Volksen, *Macromolecules*, **1995**, *28*, 4970–4974.
7. Ghiasuddin, M. Akram, M. Adeel, M. Khalid, M. N. Tahir, M. U. Khan, M. A. Asghar and M. Iqbal, *J. Mol. Struct*., **2018**, *1160*, 129–141.
8. B. Türkkan, B. Ülküseven and E. Eroğlu, *Phosphorus Sulfur Silicon Relat. Elem.*, **2014**, *190*, 53–65.
9. R. Santhakumari, K. Ramamurthi, G. Vasuki, B. M. Yamin and G. Bhagavannarayana, *Spectrochim. Acta A Mol. Biomol. Spectrosc.* **2010**, *76*, 369–375.
10. J. Edler, R. Pfister, V. Pouthier, C. Falvo and P. Hamm, *Phys. Rev. Lett.*, **2004**, *93*, 106405.
11. I. Yalçin, E. Şener, O. Özden, S. Özden and A. Akin, *Eur. J. Med. Chem.*, **1990**, *25*, 705–708.
12. V. V. Bon, S. I. Orysyk, V. I. Pekhnyo and S. V. Volkov, *J. Mol. Struct.*, **2010**, *984*, 15–22.
13. M. Imran, M. Khalid, R. Jawaria, A. Ali, M. A. Asghar, Z. Shafiq, M. A. Assiri, H. M. Lodhi and A. A. C. Braga, *ACS Omega*, **2020**, *6*, 33914–33922.
14. C. M. Reis, D. S. Pereira, R. O. Paiva, L. F. Kneipp and A. Echevarria, *Molecules*, **2011**, *16*, 10668–10684.
15. A. A. Hassan, A. A. Aly, K. M. A. El-Shaieb, T. M. I. Bedair, S. Bräse and A. B. Brown, *J. Heterocyclic Chem.*, **2013**, *51*, 674–682.
16. M. Serda, J. G. Malecki, A. Mrozek-Wilczkiewicz, R. Musiol and J. Polanski, *J. Mol. Struct.*, **2013**, *1037*, 63–72.
17. Z. Afrasiabi, E. Sinn, J. Chen, Y. Ma, A. L. Rheingold, L. N. Zakharov, N. Rath and S. Padhye, *Inorganica Chimica Acta*, **2004**, *357*, 271–278.
18. J. Chen, Y. Huang, G. Liu, Z. Afrasiabi, E. Sinn, S. Padhye and Y. Ma, *Toxicol. Appl. Pharmacol.*, **2004**, *197*, 40–48.
19. G. A. Evingur and O. Pekcan, *Comp. Struct.*, **2018**, *183*, 212–215.
20. P. Makuła, M. Pacia, and W. Macyk, *J. Phys. Chem. Lett.*, **2018**, *9*, 6814–6817.
21. T. A. Yousef, G. M. Abu El-Reash, O. A. El-Gammal and R. A. Bedier, *J. Mol. Struct.*, **2013**, *1035*, 307–317.
22. P. J. Stephens, F. J. Devlin, C. F. Chabalowski and M. J. Frisch, *J. Phys. Chem.*, **1994**, *98*, 11623–11627.
23. R. C. Binning and L. A. Curtiss, *J. Comput. Chem.*, **1990**, *11*,1206–1216.
24. R. Krishnan, J. S. Binkley, R. Seeger and J. A. Pople, *J. Chem. Phys.*, **1980**, *72*, 650.
25. A. D. McLean and G. S. Chandler, *J. Chem. Phys.*, **1980**, *72*, 5639.
26. C. Adamo and V. Barone, *J. Chem. Phys.*, **1999**, *110*, 6158.
27. T. Yanai, D. P. Tew and N.C. Handy, *Chem. Phys. Lett.*, **2004**, *393*, 51–57.
28. D. J. Chai and M. Head-Gordon, *J. Chem. Phys.*, **2008**, *128*, 084106.
29. E. G. Hohenstein, S. T. Chill and C. D. Sherrill, *J. Chem. Theory Comput.*, **2008**, *4*, 1996–2000.
30. Y. Zhao and D. G. Truhlar, *Acc. Chem. Res.*, **2008**, *41*, 157–167.
31. D. Hadji and B. Champagne, *Chemistry Africa*, **2019**, *2*, 443–453.
32. D. R. Kanis, M. A. Ranter and T. J. Marks, *Chem. Rev.*, **1994**, *94*, 195.
33. T. Verbiest, K. Clays and V. Rodriguez, "Second-order nonlinear optical characterization techniques", CRC Press, 2009.
34. R. Bersohn, Y. H. Pao and H. L. Frisch, *J. Chem. Phys.*, **1966**, *45*, 3184.
35. M. Khalid, R. Jawaria, M. U. Khan, A. A. C. Braga, Z. Shafiq, M. Imran, H. M. A. Zafar and A. Irfan, *ACS Omega*, **2021**, *6*, 16058–16065.
36. H. Reis, M. G. Papadopoulos and R. W. Munn, *J. Chem. Phys.*, **1998**, *109*, 6828.
37. D. Hadji and H. Brahim, *Theor. Chem. Acc.*, **2018**, *137*, 180.
38. T. Bensafi, D. Hadji, A. Yahiaoui, K. Argoub, A. Hachemaoui, A. Kenane, B. Baroudi, K. Toubal, A. Djafri and A. M. Benkouider, *J. Sulf. Chem.*, **2020**, *2*, 645.
39. B. Baroudi, K. Argoub, D. Hadji, A. M. Benkouider, K. Toubal, A. Yahiaoui and A. Djafri, *J. Sulfur Chem.*, **2020**, *41*, 310–325.
40. A. Mermer and S. Alyar, *Chem. Biol. Interact.*, **2022**, *351*, 109742.
41. M. Raja, R. R. Muhamed, S. Muthu and M. Suresh, *J. Mol. Struct.*, **2017**, *1128*, 481–492.
42. P. N. Prasad and D. J. Williams, "Introduction to nonlinear optical effects in organic molecules and polymers", John Wiley, New York, 1991, p. 1.
43. M. Muthukkumar, T. Bhuvaneswari, G. Venkatesh, C. Kamal, P.Vennila, S. Armaković, S. J. Armaković, Y. S. Mary and C. Y. Panicker, *J. Mol. Liq.*, **2018**, *272*, 481–495.
44. N. S. Labidia, A. Djebailib and I. Rouina, *J. Saudi Chem. Soc.*, **2011**, *15*, 29–37.
45. J. L Oudar and J. Zyss, *Phys. Rev. A*, **1982**, *26*, 2028.
46. B. T. Rajeswari, P. Sathya, P. Dhanasekaran, G. Vinitha, S. Meyvel, V. Vijayalakshmi and J. Aarthi, *J. Mater. Sci: Mater. Electron.*, **2021**, *32*, 22984–22998.
47. A. Merouane, A. Mostefai, D. Hadji, A. Rahmouni, M. Bouchekara, A. Ramdani and S. Taleb, *Monatsh. Chem.*, **2020**, *151*, 1095.
48. D. Hadji, *Mater. Chem. Phys.*, **2021**, *262*, 124280.
49. D. Hadji and A. Rahmouni, *J. Mol. Struct.*, **2016**, *1106*, 343.
50. M. Boukabene, H. Brahim, D. Hadji and A. Guendouzi, *Theor. Chem. Acc.*, **2020**, *139*, 48.
51. M. Basharat, Y. Abbas, D. Hadji, Z. Ali, S. Zhang, H. Ma, Z. Wu and W. Liu, *J. Mater. Chem. C*, **2020**, *8*, 13612–13620.
52. D. Hadji, B. Haddad, S. A. Brandán, S.K. Panja, A. Paolonee, M. Drai, D. Villemin, S. Bresson and M. Rahmouni, *J. Mol. Struct.*, **2020**, *1220*, 128713.
53. A. Benmohammed, D. Hadji, A. Guendouzi, Y. Mouchaal, A. Djafri and A. Khelil, *J. Elec. Materi.*, **2021**, *50*, 5282.
54. R. Gheribi, D. Hadji, R. Ghallab, M. Medjani, M. Benslimane, C. Trifa, G. Dénès and H. Merazig, *J. Mol. Struct.*, **2021**, *1248*, 131392.
55. Y. Bekki, D. Hadji, A. Guendouzi, B. Houari and M. Elkeurti, *Chem. Data Collect.*, **2021**, *37*, 100809.
56. R. Basri, M. Khalid, Z. Shafiq, M. S. Tahir, S. M. U. Khan, M. N. Tahir, M. M. Naseer, A. Tahir, M. U. Khan, M. N. Tahir, M. M. Naseer and A. A. C. Braga, *ACS Omega*, **2020**, *5*, 30176–30188.
57. M. Li, Y. Bai, B. Zhang, C. Duan, J. Xu and Q. Meng, *Inorg. Chem.*, **2005**, *44*, 5459–5466.
58. R. Jawaria, M. Hussain, M. Khalid, M. U. Khan, M. N. Tahir, M.M. Naseer, A. A. C. Braga and Z. Shafiq, *Inorganica Chim. Acta*, **2019**, *486*, 162–171.